Low-loss fs-laser-written surface waveguide lasers at >2 μm in monoclinic Tm^{3+}:$MgWO_4$

Esrom Kifle,[1] Pavel Loiko,[2] Javier Rodríguez Vázquez de Aldana,[3] Carolina Romero,[3] Víctor Llamas,[1,4] Josep Maria Serres,[1,4] Magdalena Aguiló,[1] Francesc Díaz,[1] Lizhen Zhang,[5] Zhoubin Lin,[5] Haifeng Lin,[5] Ge Zhang,[5] Viktor Zakharov,[6] Andrey Veniaminov,[6] Valentin Petrov,[7] Uwe Griebner,[7] Xavier Mateos,[1,*] Li Wang[7] and Weidong Chen[5,7]

[1]Universitat Rovira i Virgili (URV), Física i Cristal·lografia de Materials i Nanomaterials (FiCMA-FiCNA)-EMaS, Marcel.li Domingo 1, 43007 Tarragona, Spain
[2]Centre de Recherche sur les Ions, les Matériaux et la Photonique (CIMAP), UMR 6252 CEA-CNRS-ENSICAEN, Université de Caen Normandie, 6 Boulevard du Maréchal Juin, 14050 Caen Cedex 4, France
[3]Aplicaciones del Láser y Fotónica, University of Salamanca, 37008 Salamanca, Spain
[4]Eurecat, Centre Tecnològic de Catalunya, Unitat Advanced Manufacturing Systems (AMS), Campus Sescelades, 43007 Tarragona, Spain
[5]Key Laboratory of Optoelectronic Materials Chemistry and Physics, Fujian Institute of Research on the Structure of Matter, Chinese Academy of Sciences, Fuzhou, 350002 Fujian, China
[6]ITMO University, 49 Kronverkskiy Pr., 197101 St. Petersburg, Russia
[7]Max Born Institute for Nonlinear Optics and Short Pulse Spectroscopy, 2A Max-Born-Str., 12489 Berlin, Germany
**Corresponding author: xavier.mateos@urv.cat*

Received XX Month XXXX; revised XX Month, XXXX; accepted XX Month XXXX; posted XX Month XXXX (Doc. ID XXXXX); published XX Month XXXX

Surface channel waveguides (WGs) based on a half-ring (40–60-μm diameter) depressed-index cladding (type III) geometry are fabricated in monoclinic Tm^{3+}:$MgWO_4$ by femtosecond laser writing at a repetition rate of 1 kHz. The WGs are characterized by confocal laser microscopy and μ-Raman spectroscopy. A Tm^{3+}:$MgWO_4$ WG laser generates 320 mW at ~2.02 μm with a slope efficiency of 64.4%. The WG emits a transverse single-mode and linear polarization (E || N_m). A remarkable low-loss of <0.1 dB/cm is measured for the WG. Vibronic laser emission at ~2.08 μm is also achieved.

http://dx.doi.org/10.1364/OL.99.099999

Magnesium monotungstate ($MgWO_4$) has been recognized recently as an excellent host material for doping with trivalent thulium ions (Tm^{3+}) [1,2]. It belongs to the monoclinic crystal class (sp. gr. C^4_{2h} – $P2/c$, wolframite, [Fe,Mn]WO_4, type structure) [3] and shows a single crystallographic site for Tm^{3+} ions (the Mg^{2+} one, symmetry: C_2). Charge compensation for the heterovalent doping is provided by univalent alkali-metal cations (e.g., Na^+) in the flux [4]. $MgWO_4$ exhibits good thermo-mechanical properties, such as high thermal conductivity $\langle\kappa\rangle$ = 8.7 $Wm^{-1}K^{-1}$ [5] and low anisotropy of the thermal expansion, α_a = 11.22, α_b = 8.09 and α_c = 8.77 [10^{-6} K^{-1}] [4], leading to promising power scaling capabilities.

For Tm^{3+} ions (electronic configuration: [Xe]$4f^{12}$), $MgWO_4$ shows attractive spectroscopic properties, i.e., intense and broad emission bands for the $^3F_4 \rightarrow {}^3H_6$ transition with polarized light, and large Stark splitting of the ground-state, $\Delta E(^3H_6)$ = 633 cm^{-1} [6]. Thus, the broad polarized emission bands of Tm^{3+}:$MgWO_4$ extend well above 2 μm avoiding the structured water vapor atmospheric absorption. The latter is a key issue for the generation of femtosecond pulses in mode-locked (ML) lasers in the 2 μm spectral range [7]. It was recently confirmed by a graphene ML Tm^{3+}:$MgWO_4$ laser which generated 86 fs pulses at a wavelength of 2017 nm (bandwidth: 53 nm) at a repetition rate of 87 MHz [2]. Furthermore, continuous wavelength tuning was achieved from 1897 to 2062 nm [2]. As $MgWO_4$ is an efficient Raman-active material, laser emission at even longer wavelengths (up to 2093 nm) was realized due to the electron-phonon coupling [6]. A continuous-wave (CW) Tm^{3+}:$MgWO_4$ laser generated 3.09 W at 2022-2034 nm with a slope efficiency as high as 50% [1].

Due to its attractive thermal and spectroscopic properties, Tm^{3+}:$MgWO_4$ is also promising for ML waveguide (WG) lasers above 2 μm. While Tm^{3+}-doped monoclinic double tungstate (MDT) bulk crystals have been widely explored to this aim [8], WG laser operation has never been demonstrated with monoclinic divalent-metal monotungstates. In the present work, we

demonstrate the first Tm^{3+}:$MgWO_4$ WG laser featuring low passive losses and high laser efficiency, as a first step towards high-repetition-rate (GHz-range) ML WG lasers [9].

As a fabrication method, we selected femtosecond Direct Laser Writing (fs-DLW). This method is based on focusing a fs laser beam inside a small volume (few μm^3) within a transparent material resulting in partial amorphization of the damaged area leading to a permanent refractive index variation ($\Delta n > 0$ or $\Delta n < 0$) [10]. The advantages of fs-DLW are: short interaction time and high precision, single step procedure, suitability for various materials *incl.* anisotropic crystals, variable WG geometries, moderate to low propagation losses. Efficient fs-DLW thulium WG lasers have been demonstrated [11,12]. Lancaster *et al.* reported on a buried channel WG laser inscribed in a Tm^{3+}:ZBLAN glass delivering 205 mW at ~1.89 μm with a slope efficiency η of 67% and low passive losses δ_{loss} of 0.4±0.2 dB/cm [11]. Kifle *et al.* demonstrated a surface WG laser in a Tm^{3+}:$KLu(WO_4)_2$ crystal generating 171 mW at ~1.85 μm with η = 38% and δ_{loss} = 0.7±0.3 dB/cm [12].

The Tm^{3+}:$MgWO_4$ crystal was grown by the Top-Seeded Solution Growth (TSSG) method using Na_2WO_4 as a solvent [13]. The Tm^{3+} doping level was 0.89 at.% (N_{Tm} = 1.41×10^{20} cm^{-3}). A rectangular sample with dimensions 1.86(N_g)×3.96(N_m)×3.05(N_p) mm^3 was cut and polished along the optical indicatrix frame of this biaxial crystal [6]. The DLW was performed using 120-fs pulses with a central wavelength of 795 nm from a Ti:Sapphire regenerative amplifier at a repetition rate of 1 kHz. A small portion of the pulse energy (86 nJ, measured after the focusing optics) was employed with polarization $\boldsymbol{E} \parallel N_m$. The fs radiation was focused into the crystal along the N_g–axis through the top surface using a 40× microscope objective (N.A. = 0.65). The sample was translated at a speed of 400 μm/s along the N_p-axis producing damage tracks.

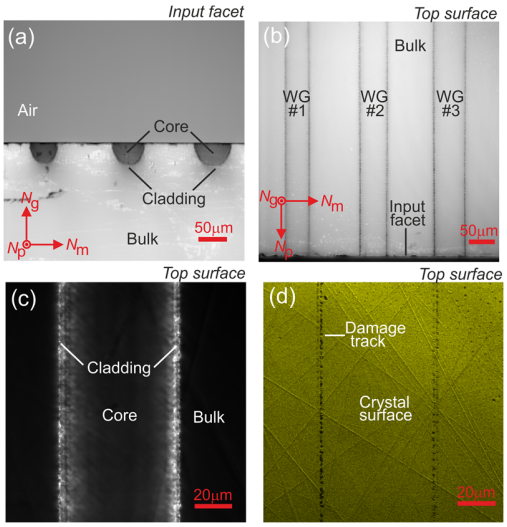

Fig. 1. Confocal microscopy study of fs-DLW surface channel WGs in Tm^{3+}:$MgWO_4$: (a) end-facet view, transmission mode, polarized light (P || N_g); (b,c) top surface view, transmission mode: (b) a general view in polarized light (P || N_p); (c) a close look on the 60 μm WG in crossed polarizers (P || N_p, A || N_m); (d) the same area as in (c) in reflection mode. λ = 405 nm. P – polarizer, A – analyzer.

Surface channel WGs with a half-ring depressed-index cladding ($\Delta n > 0$, classified as type III microstructures [10]) were produced. Their geometry was studied using a confocal scanning laser microscope LSM 710 (Carl Zeiss) equipped with a polarizer (P), an analyzer (A), a blue GaN laser (405 nm), and a 20× objective (N.A. = 0.75), Fig. 1(a). The spatial resolution was 0.24 μm. The diameter of the cladding was 40, 50 or 60 μm. The inner part of the guides appeared to be darker than the surrounding bulk area due to light scattering at the curved cladding (the waveguiding conditions are not satisfied at high N.A. of the objective). The axis of the WG was located at 20-30 μm beneath the top surface. Except of the damage tracks no cracks in the writing areas nor in the bulk volume were observed. The damage tracks passed continuously through the whole length of the 3.05 mm long sample (along the N_p-axis), Fig. 1(b). The study of the sample in crossed polarizers (P and A) revealed bright areas localized at the damage tracks indicating a local alteration of the size and orientation of the optical indicatrix, Fig. 1(c). The damage tracks reached the top surface, Fig. 1(d), producing a shallow ablation groove at the external tracks.

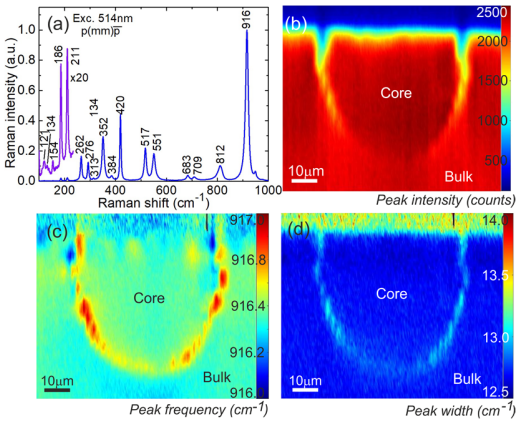

Fig. 2. Micro-Raman mapping of the fs-DLW surface channel WG (size: 50 μm) in Tm^{3+}:$MgWO_4$: (a) polarized Raman spectrum for the $p(mm)\bar{p}$ geometry, numbers denote the Raman frequencies in cm^{-1}, λ_{exc} = 514 nm; (b-d) maps of the crystal end-facet representing the variation of (b) peak Raman intensity, (c) peak frequency and (d) peak width (FWHM) for the ~916 cm^{-1} Raman band.

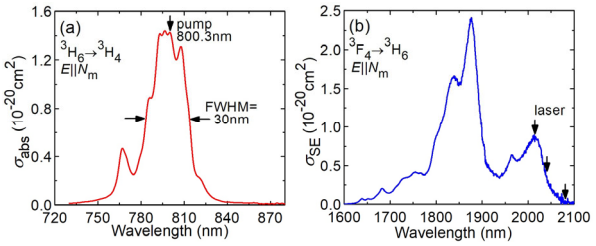

Fig. 3. Spectroscopy of Tm^{3+} ions in monoclinic $MgWO_4$: (a) absorption cross-section, σ_{abs}, for the $^3H_6 \rightarrow {}^3H_4$ transition, and (b) stimulated-emission (SE) cross-section, σ_{SE}, for the $^3F_4 \rightarrow {}^3H_6$ transition. The light polarization is $\boldsymbol{E} \parallel N_m$. The vertical *arrows* in (a),(b) indicate the pump and emission wavelengths for the waveguide laser, respectively.

Raman spectroscopy is a sensitive tool to study the structure alteration at the μ-scale [14]. The polarized Raman spectrum of the Tm^{3+}:$MgWO_4$ crystal for the $p(mm)\bar{p}$ geometry (Porto's notations)

is shown in Fig. 2(a). The most intense Raman band denoted as $\nu_1(A_{1g})$ is observed at ~916 cm^{-1} and assigned to symmetric stretching W – O vibrations in the [WO_6] octahedra [13]. The peak intensity, width (FWHM) and position were monitored over the sample end-facet resulting in μ-Raman maps, Fig. 2(c-d). In the damaged regions, a drop of intensity, broadening of the band and its shift to longer frequencies are observed indicating a reduction of crystallinity (a partial amorphization). The crystalline quality of the core is well preserved as manifested by the almost unchanged Raman response with respect to the bulk regions.

In Tm^{3+}:$MgWO_4$, the maximum absorption cross-section, σ_{abs}, for the $^3H_6 \rightarrow {}^3H_4$ pump transition is 1.43×10^{-20} cm^2 at 800.3 nm, Fig. 3(a). The peak stimulated-emission (SE) cross-section, σ_{SE}, at wavelengths >2 μm where the laser operation is expected, is 0.85×10^{-20} cm^2 at 2015 nm, Fig. 3(b). Both values are specified for $\boldsymbol{E} \parallel N_m$. The upper laser level ($^3F_4$) lifetime is 1.93 ms [13].

The laser cavity comprised a flat pump mirror coated for high transmission, HT (T = 96%) at 0.80 μm and for high reflection, HR at 1.80-2.06 μm, and a set of flat output couplers (OCs) having a transmission T_{OC} = 1.5-30% at the laser wavelength. We also used a special bandpass OC coated for HT at <2 μm and providing T_{OC} = 1.6% at >2.05 μm. All the OCs provided HR at ~0.80 μm, so the WG was pumped in a double-pass. The crystal was mounted on a passively cooled BK7 glass block and placed between the cavity mirrors without index-matching among them. The mirrors were gently pressed towards the WG endfaces resulting in a geometrical cavity length of ~3.1 mm.

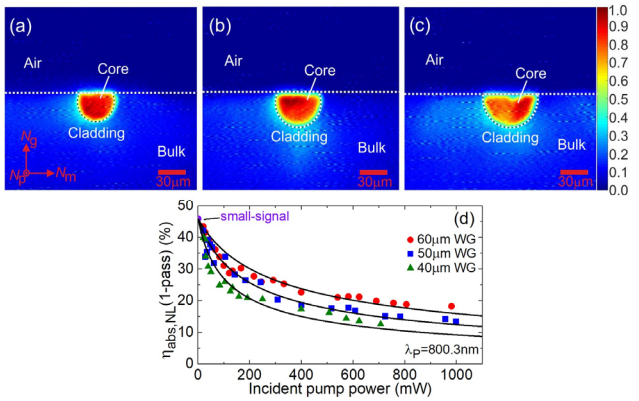

Fig. 4. (a-c) Pump modes at the output facet of the fs-DLW WGs in Tm^{3+}:$MgWO_4$: the WG cladding diameters are (a) 40 μm, (b) 50 μm and (c) 60 μm. *White dashed lines* indicate the WG cladding and the air/crystal interfaces. The pump polarization ($\boldsymbol{E} \parallel N_m$) is horizontal; (d) measured single-pass pump absorption in the WGs under non-lasing conditions, $\eta_{abs,NL}$: *symbols* – experimental data, *curve* – simulation with a rate-equation model. The pump wavelength is 800.3 nm.

The pump power from a CW Ti:Sapphire laser was up to ~2 W at 800.3 nm ($M^2 \approx 1$). The pump, polarized with $\boldsymbol{E} \parallel N_m$ (in the crystal), was focused using a 10× microscope objective (N.A. = 0.28, f = 20 mm, T = 75% at 0.80 μm) to a spot with a diameter of 25±5 μm. The pump coupling efficiency, η_{coupl}, was estimated to be 88.4±1% from pump-transmission measurements at 830 nm. The pump is confined in the slightly D-shaped cladding profile; no leakage into the bulk was detected, Fig. 4(a). The single-pass pump absorption under non-lasing conditions, $\eta_{abs,NL}$, determined at 800.3 nm by the end-fire method, gradually decreased with the incident pump power P_{inc} due to the ground-state bleaching. This effect was enhanced for smaller cladding diameters. The absorbed pump power P_{abs} was determined from $\eta_{abs,NL}$ at the threshold power for each OC and accounting for double-pass pumping.

The input-output characteristics for the 60 μm WG are shown in Fig. 5(a). Exceptionally for the best-performing T_{OC} = 3%, we removed the optical elements placed to attenuate P_{inc} resulting in higher pump power. The laser generated 320 mW at ~2015 and 2036 nm with a slope efficiency η of 64.4% (vs. P_{abs}). The laser threshold was at P_{abs} = 126 mW and the optical-to-optical efficiency at the maximum pump level was 24.7% (vs. P_{inc}). The total pump absorption (in two passes) was 48.1%. The laser slope efficiency slightly increased with the output coupling, reaching η = 69.3% for T_{OC} = 20%. The laser threshold decreased for smaller T_{OC}, from 186 mW (30% OC) down to 117 mW (1.5% OC). No thermal roll-over in the output dependences was detected at least until P_{abs} = 0.6 W; the power scaling was limited by the available pump. The laser operated for tens of minutes without a significant decrease of the output power.

The polarization of the laser emission was linear ($\boldsymbol{E} \parallel N_m$), naturally selected by the strong anisotropy of the gain in Tm^{3+}:$MgWO_4$. The laser spectra are shown in Fig. 5(b). For small T_{OC} < 9%, the emission occurred at ~2.02 and 2.04 μm. For higher output coupling (9-30%), only the short-wavelength emission was supported due to the quasi-three-level nature of the $^3F_4 \rightarrow {}^3H_6$ Tm^{3+} laser scheme, i.e., influenced by reabsorption.

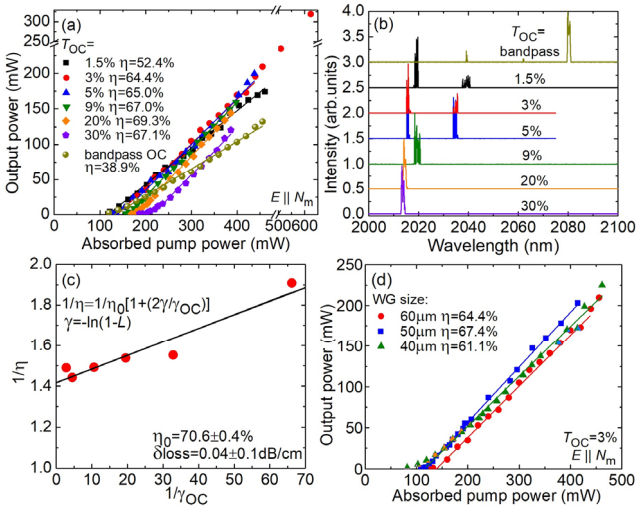

Fig. 5. (a-c) Fs-DLW Tm^{3+}:$MgWO_4$ surface channel WG (60 μm) laser: (a) input-output dependences, η – slope efficiency; (b) laser emission spectra measured at the maximum P_{abs}; (c) Caird analysis: the plot of inverse of the slope efficiency, $1/\eta$, vs. inverse of the output-coupling loss, $1/\gamma_{OC}$, $\gamma_{OC} = -\ln(1 - T_{OC})$; (d) Comparison of the output performance of WGs with cladding diameters of 40 – 60 μm: η – slope efficiency, T_{OC} = 3%. The laser polarization is $\boldsymbol{E} \parallel N_m$.

The passive losses in the 60 μm WG were estimated using the Caird analysis [15], Fig. 5(c). The resulting internal slope efficiency was η_0 = 70.6±0.4% and δ_{loss} = 0.04+0.1 dB/cm. This value is well below of those reported previously for fs-DLW WGs in Tm^{3+}:ZBLAN glass (0.4±0.2 dB/cm) [11]. Moreover, the passive

loss is comparable with the best reports on surface channel (ridge) WGs in Tm^{3+}:MDT single-crystalline films fabricated by Liquid Phase Epitaxy (LPE) and Ar^+ ion beam milling (<0.11 dB/cm) [16].

We intentionally studied the laser performance employing the bandpass OC, Fig. 5(a,b, dark green). The laser exhibited a low laser threshold of 120 mW and generated 132 mW at ~2080 nm with η = 38.9%. This wavelength is well beyond the limit for the purely electronic $^3F_4 \rightarrow {}^3H_6$ Tm^{3+} transition in $MgWO_4$ (2017 nm, between the Stark sub-levels with the energies 5591 cm^{-1} ($^3F_4$) and 633 cm^{-1} ($^3H_6$) [6]), i.e., the first demonstration of a vibronic WG laser. It is assigned to the electron-phonon coupling between the electronic transitions of Tm^{3+} and the low-frequency Raman modes of the host [17], Fig. 2(a), such as 121 (A_g), 134 or 154 (both B_g) cm^{-1}.

The performance of the surface WG lasers with different size of the cladding (40-60 μm) is compared in Fig. 5(d). The slope efficiency was similar for all the studied guides while the laser threshold clearly decreased for smaller cladding diameter: it amounted to 108 mW (50 μm WG) and 82 mW (40 μm WG), both for T_{OC} = 3%. The laser polarization for all the WGs was $\boldsymbol{E} \parallel N_m$.

All the studied WG lasers operated in the fundamental transverse mode. The latter might benefit from additional mode "filtering" provided by the reabsorption (gain-guiding) [18]. An example of the mode for the 40 μm WG is shown in Fig. 6(a). It is well confined within the WG cladding. The 1D intensity profiles, Fig. 6(b), are well fitted to a Gaussian distribution (goodness of the fit: $R^2 > 0.99$) yielding mode diameters $2w_L$ ($\parallel N_g$) = 27.2 μm and $2w_L$ ($\parallel N_m$) = 24.5 μm. The mode ellipticity is weak (e = 1.11).

The numerical aperture (N.A.) of the guides was estimated by measuring the divergence of the laser beam θ (half-angle) as N.A. = $\sin\theta$. It was similar along the vertical and horizontal directions, N.A. = 0.082 and 0.087±0.005, respectively. Within the approximation of a set-index guide, $N.A.^2 \approx 2n_{core}\Delta n$, one obtains $\Delta n = n_{cladding} - n_{core}$ of about -1.7×10^{-3} (here, n_{core} ~2.03 for $\boldsymbol{E} \parallel N_m$ [6]). A similar value was reported for Tm^{3+}:ZBLAN glass ($\Delta n \sim -1.5\times10^{-3}$) [11].

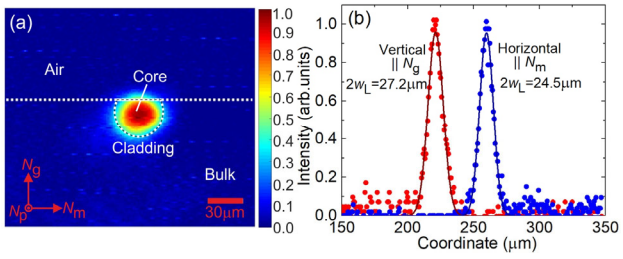

Fig. 6. (a) Spatial near-field laser mode profile of the 40 μm WG fabricated by fs-DLW in Tm^{3+}:$MgWO_4$. P_{abs} = 0.4 W, T_{OC} = 9%. The laser polarization is horizontal ($\boldsymbol{E} \parallel N_m$). *White lines* indicate the WG cladding and the air / crystal interfaces; they are drawn as guides for the eye; (b) 1D intensity plots of the intensity profile: *symbols* – experimental points, *curves* – their Gaussian fits.

To conclude, the monoclinic crystal Tm^{3+}:$MgWO_4$ is promising for highly-efficient low-loss (<0.1 dB/cm) fs-DLW waveguide lasers at wavelength above 2 μm, due to its attractive spectroscopic, vibronic and thermal properties. In the present work, we achieved the highest slope efficiency (69.3%) and output power (320 mW) for any thulium waveguide laser fabricated by femtosecond direct laser writing. Furthermore, the first "vibronic" Tm waveguide laser with the longest emission wavelength of 2080 nm for Tm-doped WGs is also demonstrated. The designed photonic micro-structures with a size in the few millimeter range are highly attractive for the generation of ultrashort pulses in compact ML lasers operating at high repetition rates (GHz-range), as well as for surface activation, e.g., leading to pulsed operation via evanescent-field coupling.

Funding. Spanish Government (MAT2016-75716-C2-1-R (AEI/FEDER,UE), FIS2017-87970-R); Generalitat de Catalunya (2017SGR755); Junta de Castilla y León (SA287P18); National Natural Science Foundation of China (61975208, 51761135115, 61850410533, 61575199, 61875199); Ministry of Science and Higher Education of the Russian Federation (Goszadanie 2019-1080); Deutsche Forschungsgemeinschaft (PE 607/14-1).

Acknowledgments. Víctor Llamas is a fellow of Eurecat's "Vicente López" PhD grant program.

Disclosures. The authors declare no conflicts of interest.

References

1. P. Loiko, J. M. Serres, X. Mateos, M. Aguiló, F. Díaz, L. Zhang, Z. Lin, H. Lin, G. Zhang, K. Yumashev, V. Petrov, U. Griebner, Y. Wang, S. Y. Choi, F. Rotermund, and W. Chen, Opt. Lett. **42**, 1177 (2017).
2. Y. Wang, W. Chen, M. Mero, L. Zhang, H. Lin, Z. Lin, G. Zhang, F. Rotermund, Y. J. Cho, P. Loiko, X. Mateos, U. Griebner, and V. Petrov, Opt. Lett. **42**, 3076 (2017).
3. V. B. Kravchenko, J. Struct. Chem. **10**, 139 (1969).
4. L. Zhang, P. Loiko, J.M. Serres, E. Kifle, H. Lin, G. Zhang, E. Vilejshikova, E. Dunina, A. Kornienko, L. Fomicheva, U.Griebner, V. Petrov, Z. Lin, W. Chen, K. Subbotin, M. Aguiló, F. Díaz, and X. Mateos, J. Lumin. **213**, 316 (2019).
5. L. Zhang, Y. Huang, S. Sun, F. Yuan, Z. Lin, and G. Wang, J. Lumin. **169**, 161 (2016).
6. P. Loiko, L. Zhang, J.M. Serres, Y. Wang, M. Aguiló, F. Díaz, Z. Lin, H. Lin, G. Zhang, E. Vilejshikova, E. Dunina, A. Kornienko, L. Fomicheva, V. Petrov, U. Griebner, W. Chen, and X. Mateos, J. Alloys Compd. **763**, 581 (2018).
7. Y. Wang, G. Xie, X. Xu, J. Di, Z. Qin, S. Suomalainen, M. Guina, A. Härkönen, A. Agnesi, U. Griebner, X. Mateos, P. Loiko, and V. Petrov, Opt. Mater. Express **6**, 131 (2016).
8. K. van Dalfsen, S. Aravazhi, C. Grivas, S. M. García-Blanco, and M. Pollnau, Opt. Lett. **39**, 4380 (2014).
9. A. G. Okhrimchuk and P.A. Obraztsov, Sci. Rep. **5**, 11172 (2015).
10. F. Chen and J. R. Vázquez de Aldana, Laser Photonics Rev. **8**, 251 (2014).
11. D. G. Lancaster, S. Gross, A. Fuerbach, H. E. Heidepriem, T. M. Monro, and M. J. Withford, Opt. Express **20**, 27503 (2012).
12. E. Kifle, P. Loiko, J. R. V. de Aldana, C. Romero, A. Ródenas, S. Y. Choi, J. E. Bae, F. Rotermund, V. Zakharov, A. Veniaminov, M. Aguiló, F. Díaz, U. Griebner, V. Petrov, and X. Mateos, Photon. Res. **6**, 971 (2018).
13. L. Zhang, H. Lin, G. Zhang, X. Mateos, J. M. Serres, M. Aguiló, F. Díaz, U. Griebner, V. Petrov, Y. Wang, P. Loiko, E. Vilejshikova, K. Yumashev, Z. Lin, and W. Chen, Opt. Express **25**, 3682 (2017).
14. A. Ródenas, A. H. Nejadmalayeri, D. Jaque, and P. Herman, Opt. Express **16**, 13979 (2008).
15. J. A. Caird, S. A. Payne, P. R. Staber, A. J. Ramponi, L. L. Chase, and W. F. Krupke, IEEE J. Quantum Electron. **24**, 1077 (1988).
16. K. van Dalfsen, S. Aravazhi, D. Geskus, K. Wörhoff, and M. Pollnau, Opt. Express **19**, 5277 (2011).
17. P. Loiko, X. Mateos, S. Y. Choi, F. Rotermund, J. M. Serres, M. Aguiló, F. Díaz, K. Yumashev, U. Griebner, and V. Petrov, J. Opt. Soc. Am. B. **33**, D19 (2016).
18. J. I. Mackenzie, S. C. Mitchell, R. J. Beach, H. E. Meissner, and D. P. Shepherd, Electron. Lett. **37**, 898 (2001).

References

1. P. Loiko, J. M. Serres, X. Mateos, M. Aguiló, F. Díaz, L. Zhang, Z. Lin, H. Lin, G. Zhang, K. Yumashev, V. Petrov, U. Griebner, Y. Wang, S. Y. Choi, F. Rotermund, and W. Chen, "Monoclinic Tm^{3+}:$MgWO_4$: a promising crystal for continuous-wave and passively Q-switched lasers at ~2 μm," Opt. Lett. **42**(6), 1177-1180 (2017).
2. Y. Wang, W. Chen, M. Mero, L. Zhang, H. Lin, Z. Lin, G. Zhang, F. Rotermund, Y. J. Cho, P. Loiko, X. Mateos, U. Griebner, and V. Petrov, "Sub-100 fs Tm:$MgWO_4$ laser at 2017 nm mode locked by a graphene saturable absorber," Opt. Lett. **42**(16), 3076-3079 (2017).
3. V. B. Kravchenko, "Crystal structure of the monoclinic form of magnesium tungstate $MgWO_4$," J. Struct. Chem. **10**(1), 139-140 (1969).
4. L. Zhang, P. Loiko, J.M. Serres, E. Kifle, H. Lin, G. Zhang, E. Vilejshikova, E. Dunina, A. Kornienko, L. Fomicheva, U.Griebner, V. Petrov, Z. Lin, W. Chen, K. Subbotin, M. Aguiló, F. Díaz, and X. Mateos, "Growth, spectroscopy and first laser operation of monoclinic Ho^{3+}:$MgWO_4$ crystal," J. Lumin. **213**, 316-325 (2019).
5. L. Zhang, Y. Huang, S. Sun, F. Yuan, Z. Lin, and G. Wang, "Thermal and spectral characterization of Cr^{3+}:$MgWO_4$ – a promising tunable laser material, J. Lumin. 169, Part A, 161-164 (2016).
6. P. Loiko, L. Zhang, J.M. Serres, Y. Wang, M. Aguiló, F. Díaz, Z. Lin, H. Lin, G. Zhang, E. Vilejshikova, E. Dunina, A. Kornienko, L. Fomicheva, V. Petrov, U. Griebner, W. Chen, and X. Mateos, "Monoclinic Tm^{3+}:$MgWO_4$ crystal: Crystal-field analysis, tunable and vibronic laser demonstration," J. Alloys Compd. **763**, 581-591 (2018).
7. Y. Wang, G. Xie, X. Xu, J. Di, Z. Qin, S. Suomalainen, M. Guina, A. Härkönen, A. Agnesi, U. Griebner, X. Mateos, P. Loiko, and V. Petrov, "SESAM mode-locked Tm:CALGO laser at 2 μm," Opt. Mater. Express **6**(1), 131-136 (2016).
8. K. van Dalfsen, S. Aravazhi, C. Grivas, S. M. García-Blanco, and M. Pollnau, "Thulium channel waveguide laser with 1.6 W of output power and ~80% slope efficiency," Opt. Lett. **39**(15), 4380–4383 (2014).
9. A. G. Okhrimchuk and P.A. Obraztsov, "11-GHz waveguide Nd: YAG laser CW mode-locked with single-layer graphene," Sci. Rep. **5**(1), 11172 (2015).
10. F. Chen and J. R. Vázquez de Aldana, "Optical waveguides in crystalline dielectric materials produced by femtosecond-laser micromachining," Laser Photon. Rev. **8**(2), 251-275 (2014).
11. D. G. Lancaster, S. Gross, A. Fuerbach, H. E. Heidepriem, T. M. Monro, and M. J. Withford, "Versatile large-mode-area femtosecond laser-written Tm:ZBLAN glass chip lasers," Opt. Express **20**(25), 27503–27509 (2012).
12. E. Kifle, P. Loiko, J. R. V. de Aldana, C. Romero, A. Ródenas, S. Y. Choi, J. E. Bae, F. Rotermund, V. Zakharov, A. Veniaminov, M. Aguiló, F. Díaz, U. Griebner, V. Petrov, and X. Mateos, "Passively Q-switched femtosecond-laser-written thulium waveguide laser based on evanescent field interaction with carbon nanotubes," Photon. Res. **6**(10), 971-980 (2018).
13. L. Zhang, H. Lin, G. Zhang, X. Mateos, J. M. Serres, M. Aguiló, F. Díaz, U. Griebner, V. Petrov, Y. Wang, P. Loiko, E. Vilejshikova, K. Yumashev, Z. Lin, and W. Chen, "Crystal growth, optical spectroscopy and laser action of Tm^{3+}-doped monoclinic magnesium tungstate," Opt. Express **25**(4), 3682-3693 (2017).
14. A. Ródenas, A. H. Nejadmalayeri, D. Jaque, and P. Herman, "Confocal Raman imaging of optical waveguides in $LiNbO_3$ fabricated by ultrafast high-repetition rate laser-writing," Opt. Express **16**(18), 13979-13989 (2008).
15. J. A. Caird, S. A. Payne, P. R. Staber, A. J. Ramponi, L. L. Chase, and W. F. Krupke, "Quantum electronic properties of the $Na_3Ga_2Li_3F_{12}$:Cr^{3+} laser," IEEE J. Quantum Electron. **24**(6), 1077–1099 (1988).
16. K. van Dalfsen, S. Aravazhi, D. Geskus, K. Wörhoff, and M. Pollnau, "Efficient $KY_{1-x-y}Gd_xLu_y(WO_4)_2$:$Tm^{3+}$ channel waveguide lasers," Opt. Express **19**(6), 5277-5282 (2011).
17. P. Loiko, X. Mateos, S. Y. Choi, F. Rotermund, J. M. Serres, M. Aguiló, F. Díaz, K. Yumashev, U. Griebner, and V. Petrov, "Vibronic thulium laser at 2131 nm Q-switched by single-walled carbon nanotubes," J. Opt. Soc. Am. B. **33**(11), D19-D27 (2016).
18. J. I. Mackenzie, S. C. Mitchell, R. J. Beach, H. E. Meissner, and D. P. Shepherd, "15 W diode-side-pumped Tm:YAG waveguide laser at 2 μm," Electron. Lett. **37**(14), 898-899 (2001).